Biochimica et Biophysica Acta 1840 (2014) 565–576

Contents lists available at ScienceDirect

Biochimica et Biophysica Acta

journal homepage: www.elsevier.com/locate/bbagen

Physico-chemical characterization and the *in vitro* genotoxicity of medical implants metal alloy (TiAlV and CoCrMo) and polyethylene particles in human lymphocytes

Goran Gajski [a], Želimir Jelčić [b], Višnja Oreščanin [c], Marko Gerić [a], Robert Kollar [c], Vera Garaj-Vrhovac [a,*]

[a] Institute for Medical Research and Occupational Health, Mutagenesis Unit, 10000 Zagreb, Croatia
[b] PLIVA Croatia Ltd., TAPI Research and Development, 10000 Zagreb, Croatia
[c] Advanced Energy Ltd., 10000 Zagreb, Croatia

ARTICLE INFO

Article history:
Received 12 June 2013
Received in revised form 3 October 2013
Accepted 7 October 2013
Available online 17 October 2013

Keywords:
Joint replacement
Human lymphocyte
Cytogenotoxicity
Scanning electron microscope
Fractal analysis
Multifractal analysis

ABSTRACT

Background: The main objective of the present study was to investigate chemical composition and possible cyto/genotoxic potential of several medical implant materials commonly used in total hip joint replacement.
Methods: Medical implant metal alloy (Ti_6Al_4V and CoCrMo) and high density polyethylene particles were analyzed by energy dispersive X-ray spectrometry while toxicological characterization was done on human lymphocytes using multi-biomarker approach.
Results: Energy dispersive X-ray spectrometry showed that none of the elements identified deviate from the chemical composition defined by appropriate ISO standard. Toxicological characterization showed that the tested materials were non-cyto/genotoxic as determined by the comet and cytokinesis-block micronucleus (CBMN) assay. Particle morphology was found (by using scanning electron and optical microscope) as flat, sharp-edged, irregularly shaped fiber-like grains with the mean particle size less than 10 μm; this corresponds to the so-called "submicron wear". The very large surface area per wear volume enables high reactivity with surrounding media and cellular elements.
Conclusions: Although orthopedic implants proved to be non-cyto/genotoxic, in tested concentration (10 μg/ml) there is a constant need for monitoring of patients that have implanted artificial hips or other joints, to minimize the risks of any unwanted health effects.
General significance: The fractal and multifractal analyses, performed in order to evaluate the degree of particle shape effect, showed that the fractal and multifractal terms are related to the "remnant" level of the particles' toxicity especially with the cell viability (trypan blue method) and total number of nucleoplasmic bridges and nuclear buds as CBMN assay parameters.

© 2013 Elsevier B.V. All rights reserved.

1. Introduction

Human population can be exposed to a broad range of chemical and/or physical agents in environmental, occupational and medical settings. Exposure to particles containing metal from industrial and environmental pollution, as well as from wear debris from worn surgical implants has risen tremendously. Hip replacement surgery is one of the most important surgical advances of the last century. Since it was first performed in 1960, improvements in joint replacement surgical techniques and technology have greatly increased the effectiveness of total hip replacement. Each year around 500,000 people in America and another 300,000 people in Europe receive an orthopedic joint replacement and the number is still increasing. The most common is total hip joint replacement but similar surgical procedures are performed on other joints such as, the knee, shoulder, and elbow. On the world scale, approximately one million artificial hips are implanted annually [1–5].

Total hip arthroplasty is the surgical reconstruction or replacement of a malformed, degenerated or traumatized hip and is one of the most successful and cost-effective surgical interventions. For the total hip replacement a broad range of different artificial materials is used. One of the biggest problems concerning orthopedic joint replacements is particulate wear debris created from different implants used. Several types of different materials are today still used for the production of medical implants. The most common are soft-on-hard (metal-on-polyethylene, MOP) implants, with the new generation of hard-on-hard implants with metal-on-metal (MOM) and ceramic-on-ceramic (COC) articulating surfaces [4–9].

Abovementioned implants may wear over a period of several decades creating a large number of particles depending on the nature of the material they were made of. The particulate wear debris accumulates in the bone marrow and soft tissue adjacent to the worn implant and as such can lead to the undesirable outcome. Wear

* Corresponding author at: Institute for Medical Research and Occupational Health, Mutagenesis Unit, Ksaverska cesta 2, 10000 Zagreb, Croatia. Tel.: +385 1 4682 500; fax: +385 1 4673 303.
E-mail addresses: ggajski@imi.hr (G. Gajski), vgaraj@imi.hr (V. Garaj-Vrhovac).

0304-4165/$ – see front matter © 2013 Elsevier B.V. All rights reserved.
http://dx.doi.org/10.1016/j.bbagen.2013.10.015

produced in a hip implant leads to the loosening of a hip prosthesis and thus failure of the hip implant [6,7,10,11]. Particulate medical implants are known to induce an increase of chromosome aberrations in patients. Increase of chromosome aberrations in the bone marrow adjacent to the implant and an increase of chromosome translocations and aneuploidy in the peripheral blood are also noticed. The wear debris from implants may also cause DNA and chromosome damage, cytokine release and cytotoxicity in different human cells [12–17].

Since large number of patients and especially young patients are undergoing total joint replacements there is a constant need for development of new improved materials that will provide not only the best surgical outcome but will also be the safest for the patients in terms of possible adverse effects. Especially vulnerable are the young patients which will be exposed for longer period to the orthopedic materials. In the present study we investigated several medical implant materials commonly used in total hip joint replacement. Physical properties were determined by optical and scanning electron microscope (SEM) while chemical characterization of medical implant metal alloy (Ti_6Al_4V and CoCrMo) and high density polyethylene (PEHD) particles were analyzed by energy dispersive X-ray spectrometry (EDXRF) for the chemical composition. Moreover, the toxicological characterization was also done in order to investigate whether surgical particles of metal alloy and polyethylene are able to cause cytotoxic and/or genotoxic damage to human cells. Using *in vitro* model, human peripheral blood lymphocytes (HPBLs), as sensitive biomarkers of exposure, were exposed to particles of the abovementioned materials. In order to determine possible cytotoxic potential of medical implant particles differential staining with acridine orange (AO) and ethidium bromide (EtBr), and trypan blue (TB) exclusion technique were used. DNA damage was measured with the alkaline comet (SCGE) assay while possible further genotoxic activity was assayed using cytokinesis-block micronucleus (CBMN) technique. Another aim was also to try to establish the contribution of fractal indices in the quantification of cyto/genotoxicity of implant metal alloys and polyethylene particles in HPBLs. Combination of the abovementioned methods plays an important role in assessing cyto/genotoxicity with the possibility to evaluate the level of primary cell and genome damage even after short-term exposure. Presented results would be beneficial to implant manufacturers, surgeons as well as their patients.

2. Materials and methods

2.1. Chemicals

Chromosome kit P was from Euroclone (Milano, Italy); RPMI 1640 was from Invitrogen (Carlsbad, CA); acridine orange, bleomycin, cytohalasin B, ethidium bromide, histopaque, low melting point (LMP) and normal melting point (NMP) agaroses were from Sigma (St Louis, MO); heparinized vacutainer tubes were from Becton Dickinson (Franklin Lakes, NJ); Giemsa was from Merk (Darmstadt, Germany); trypan blue dye was from BDH Chemicals (Poole, UK). All other reagents used were laboratory-grade chemicals from Kemika (Zagreb, Croatia).

2.2. Chemical analysis

The samples of medical implants: ISO 5832-3, ISO 5832-4 and ISO 5834-2 were analyzed by EDXRF. All samples were irradiated by X-rays generated from X-ray tube (Oxford instruments, Abingdon, Oxfordshire, UK) with Mo anode (high voltage: 40 kV; current: 900 μA; cooling medium: air). The detection of characteristic X-ray radiation from the sample was conducted with Si drift detector — model SXD15C-150-500 (Canberra, Meriden, CT) (surface: 15 mm^2; FWHM for 5.9 keV ^{55}Fe: 145 eV; window: 13 μm Be; cooling: thermo-electrical (peltier)). The incident and emerging angles were 45°. For signal processing DSA 2000 (Canberra) was used. Spectral data were collected by Genie-2000 software (Canberra) while for spectrum deconvolution and quantitative analysis WinAxil software package (Canberra) was used. In order to obtain a good counting statistic, collecting time for alloys was 3000 s, while UHMWPE target was measured 40,000 s. Five replicate measurements per each implant were done. For quality assurance of the measurement the following NIST standard reference materials were used: SRM 173c Titanium-based alloy (6Al–4V); SRM 1242 high temperature alloy L 605 and SRM 2855 Additive elements in polyethylene.

2.3. Particle morphology

The surface structure and chemistry of the Ti_6Al_4V and CoCrMo metal alloy and PEHD particle samples were analyzed using a SEM (JEOL JSM 5800, Tokyo, Japan) with attached Oxford Instruments LINK ISIS energy dispersive X-ray analysis (EDX) system (Tubney Woods, Abingdon, Oxfordshire, UK). For SEM, a particle sample was adhered on an aluminium stub using double-sided adhesive tape, and gold coated with a sputter-coater. Identified by SEM morphology, the particles were analyzed with EDX to determine elemental composition, without gold coating. The particles were also examined at 10× magnification using an optical microscope (Olympus BX51, Tokyo, Japan).

2.4. Blood sampling and treatment

For toxicological characterization the samples of medical implants were milled in diamond based mill. Obtained particles were added into medium making the final concentration of 100 mg/l which was then sonicated at 600 Hz for 5 min.

The effects of medical implants samples (Ti_6Al_4V, CoCrMo and PEHD) were evaluated in HPBLs obtained from a two healthy male, non-smoking donors. Subjects gave informed consent to participate in this study. The study was approved by the institutional ethics committee and observed the ethical principles of the Declaration of Helsinki. According to questionnaire, which the donors completed, they had not been exposed to ionizing radiation for diagnostic or therapeutic purposes or to known genotoxic chemicals that might have interfered with the results of the testing for a year before blood sampling. Blood was drawn by antecubital venipuncture into heparinized vacutainers containing lithium heparin as anticoagulant under aseptic conditions.

The comet assay and the CBMN assay were conducted on the whole blood, while cytotoxicity was performed on isolated HPBLs. The aliquots of medical implants solution were added to the whole blood samples during 24 h period to make the final concentration of 10 μg/ml. In each experiment, a non treated control and a positive control were included. After the treatment, all experiments were conducted according to the standard protocols listed below.

2.5. Cell viability (cytotoxicity) assay

After the treatment lymphocytes were isolated by Histopaque density gradient centrifugation method [18].

2.5.1. Vital staining using acridine orange (AO) and ethidium bromide (EtBr)

Cytotoxicity was determined by differential staining with AO and EtBr and by fluorescence microscopy [19]. The slides were prepared using 200 μl of HPBLs and 2 μl of stain (AO and EtBr, both diluted in phosphate-buffered saline, PBS). A total of 100 cells per repetition were examined with an Olympus BX51 microscope (Tokyo, Japan). The cells were divided in two categories: live cells with a functional membrane and with uniform green staining of the nucleus and dead cells with uniform red staining of the nucleus.

For the vital staining using AO and EtBr blood samples were treated with 1% sodium lauryl sulfate (SLS) as a positive control.

2.5.2. Trypan blue (TB) exclusion assay

Cytotoxicity was also studied using TB exclusion technique [20]. Cells were stained with TB dye (0.4%) and were analyzed with an Olympus CX41 microscope (Tokyo, Japan). Viable (uncoloured) and dead (blue) cells were counted.

For the TB exclusion assay blood samples were treated with 1 M NaOH as a positive control.

2.6. Alkaline comet (SCGE) assay

The alkaline comet assay was carried out basically as described by Singh et al. [21] with minor modifications [22]. After the exposure to different medical implants the whole blood was mixed with 100 μl of 0.5% LMP agarose and added to fully frosted slides pre-coated with 0.6% NMP agarose. After solidifying, the slides were covered with 0.5% LMP agarose, and the cells were lysed (2.5 M NaCl, 100 mM $EDTANa_2$, 10 mM Tris, 1% sodium sarcosinate, 1% Triton X-100, 10% dimethyl sulfoxide, pH10) overnight at 4 °C. After the lysis, the slides were placed into alkaline solution (300 mM NaOH, 1 mM $EDTANa_2$, pH13) for 20 min at 4 °C to allow DNA unwinding and subsequently electrophoresed for 20 min at 1 V/cm. Finally, the slides were neutralized in 0.4 M Tris buffer (pH 7.5) for 5 min 3 times, stained with EtBr (20 μg/ml) and analyzed at 250× magnification using an epifluorescence microscope (Zeiss, Göttingen, Germany) connected through a black and white camera to an image analysis system (Comet Assay II; Perceptive Instruments Ltd., Haverhill, Suffolk, UK).

One hundred randomly captured comets from each slide were examined. To quantify DNA damage, the following comet parameters were evaluated: tail length, tail intensity (% of tail DNA), and tail moment. Tail length (*i.e.* the length of DNA migration) is related directly to the DNA fragment size and is presented in micrometers (μm). It was calculated from the center of the cell. Tail intensity is defined as the percentage of fluorescence migrated in the comet tail. Tail moment was calculated as (tail length × % of DNA in tail)/100.

For the comet assay blood samples were treated with 1 mM H_2O_2 as a positive control.

2.7. Cytokinesis-block micronucleus (CBMN) assay

The CBMN assay was carried out basically as described by Fenech and Morley [23] with minor modifications [22]. After the exposure to medical implants the whole blood (500μl) was incubated in a Euroclone medium at 37 °C in an atmosphere of 5% CO_2. Cytochalasin-B was added at a final concentration of 6 μg/ml 44 h after the culture was started. The cultures were harvested at 72 h. The lymphocytes were fixed in the methanol–acetic acid solution (3:1), air-dried and stained with 5% Giemsa solution. One thousand binuclear lymphocytes were analyzed under a light microscope (Olympus CX41, Tokyo, Japan) at 400× magnification. Micronuclei (MNi), nucleoplasmic bridges (NPBs) and nuclear buds (NBUDs) were counted in 1000 binucleated cells according to the HUMN project criteria published by Fenech et al. [24].

The nuclear division index (NDI) was determined by scoring 500 cells with one to four nuclei. The NDI was calculated using the formula $[M_1 + 2M_2 + 3(M_3 + M_4)]/1000$, where M_1–M_4 represent the number of cells with one to four nuclei, respectively, and M_3 and M_4 are equally considered to be in their third cycle [25].

For the CBMN assay blood samples were treated with 10 μg/ml bleomycin as a positive control.

2.8. Statistical analysis

For statistical evaluation Statistica 6.0 software package was used. The difference in the cell viability between control and exposed samples was done by χ^2-test, while the difference between control and hip joint samples as well as between hip joint samples for three comet assay parameters and CBMN assay parameters was assessed by Newman–Keuls test. The correlations between comet assay parameters and those obtained by CBMN assay were assessed by multiple regression analysis. $p < 0.05$ was considered significant.

2.9. Fractal analysis approaches

The problem is encountered in any attempt to categorize morphometrically the implant wear particles that the irregular structures are not easily quantifiable in geometric terms, and this is one of the reasons why the implant particle analysis has remained qualitative. Fractal geometry, however, has provided novel approaches to characterize such complex data [26]. Fractal dimension values were computed for the microscopic fine-sized texture in the SEM images of particles by the mono- and the multi-fractal approaches.

The fractal analysis method uses pixel intensity height profiles, extracted from the SEM images and presented as z-heights in an x–y image plane. The method is based on a simple principle where a square mesh of various sizes $1/\varepsilon$ is laid over the image object. Counting black, white and partially black squares separately can modify this method. The three fractal dimensions $D[BW]$ (interface surface box dimension), $D[W+BW]$ ("void" box mass dimension), and a classical box dimension $D[B+BW]$ (solid box mass dimension) are capable of describing morphological differences in particle form (HarFa software) [27]. $D[BW]$ characterizes properties of black and white boundary. Intuitively, the larger the fractal dimension, the rougher the texture is. The SEM images are not deterministic but have a statistical variation. This makes the computation of fractal dimension more difficult.

2.9.1. Multifractal approach

Multifractal methods have been found extremely useful in the analysis of images that contain layers of irregular but statistically self-similar shapes. A multifractal characterization is presented in one of two equivalent fractal dimension spectra [28]: (i) the Rényi fractal dimension spectrum, $D(q)$, or (ii) the spectrum of scaling indices [29], $f(\alpha)$, which here is called the Mandelbrot fractal dimension spectrum [28]. The Rényi fractal dimension spectrum is important because it has a geometric interpretation for positive integral q. Nice interpretations exist for subsets of the $D(q)$, in particular for the capacity dimension $q = 0$, also called the box-counting dimension, the information dimension $q = 1$, and the correlation dimension $q = 2$. The second spectrum, the Mandelbrot fractal dimension spectrum $f(\alpha)$ describes a multifractal as a union of interwoven monofractal sets, and therefore has a nicer interpretation, and also provides a functional form with compact support.

2.9.2. Spectrum of scaling indices or the Mandelbrot fractal dimension spectrum, f(α)

With multifractal analysis it is common practice to evaluate the $f(\alpha)$ spectrum [30,31]. The number of boxes $N(\alpha) = L^{-f(\alpha)}$ is given by the probability P_i of finding a white pixel within a given region i scales *as* $P_i = L^{\alpha}{}_i$ and $f(\alpha)$ may be understood as the fractal dimension of the union of regions with singularity strengths between α and $\alpha + d\alpha$. The relationship between the $D(q)$ spectrum and the $f(\alpha)$ spectrum is made via the Legendre transform:

$$f(\alpha(q)) = q \times \alpha(q) - \tau(q)$$

where $\alpha(q) = d\tau(q)/dt$ and $q\,\tau(q) = (q-1)D(q)$ is the mass correlation exponent of the q-th order. For a simple fractal, the fractal dimension is independent of q and therefore represented by a single point $f(\alpha) = \alpha = D$ on the $f(\alpha)$ spectrum.

2.9.3. Lacunarity (λ)

The lacunarity (λ) is referred in morphological analysis as gappiness, visual texture, inhomogeneity/heterogeneity, translational and rotational invariance, *etc.* Lacunarity reported here represent measures of λ based

on data gathered during overlapping scans (sliding box lacunarity) [28]. Lacunarity λ is generally based on the pixel distribution for an image, which we get from scans at different box sizes at different grid orientations, so that because λ ~ ε, there are many lacunarity values λ.

$$\lambda_{\varepsilon,g} = \left[\frac{\sigma}{\omega}\right]^2_{\varepsilon,g}$$

where σ is the standard deviation and μ is the mean for pixels per box at this size, ε, in a box count at this orientation, g. A completely homogeneous image will not vary in the pixels per box, so that the standard deviation, σ, for a box count at some ε will be 0. This means that $\lambda = 1 + (\sigma/\mu)^2 = 1$. A completely homogeneous image has a slope of 1, corresponding intuitively to the idea of no rotational or translational invariance and no gaps. The slope can be determined from the ln–ln regression line of λ over all ε, [ln(λ)/ln(ε)]. Also, in this approach a mass fractal dimension D_{MF} is calculated as: $D_{MF} = 3 - (s/2)$, where s = slope [ln ∑ I/ln ε] and for intensity I at (i,j) position for ε = (max–min)·size.

3. Results

3.1. Chemical characterisation

The basic statistical parameters for the chemical composition of three types of medical implants used as hip joint material were presented in Tables 1–3. Mean values and range concentrations for all determined parameters in all three medical implants were in agreement with ISO 5832-3, ISO 5832-4 and ISO 5834-2 certified values.

3.2. Cyotoxicity assessment

The viability of HPBLs exposed to medical implant materials for 24 h was not significantly affected determined with both assay (vital staining using AO and EtBr, and TB exclusion assay) as shown in Fig. 1A and B. Cell viability was above 94.95 ± 1.43% as determined with vital staining using AO and EtBr, and above 93.40 ± 0.28% as determined with TB exclusion assay. This is considered to be in acceptable range for conducting further genotoxic analysis [32,33] as it is very important to evaluate genotoxic potential at non-toxic concentrations to avoid false positive/negative results due to cytotoxicity and not genotoxicity.

3.3. Induction of DNA strand breaks

The whole blood was exposed to medical implant material for 24 h and the DNA damage in HPBLs was determined with the alkaline comet assay. None of the three determined parameters (tail length, tail intensity and tail moment) showed significant difference in the amount of DNA strand breaks compare to the corresponding control samples or among different hip joint materials as shown in Fig. 1C–E.

Table 1
Basic statistical parameters for elemental concentrations determined in medical implant wrought titanium 6–aluminium 4–vanadium (Ti_6Al_4V) alloy (ISO 5832-3).

Element	Statistical parameter					
	Mean	SD	RSD	Median	Minimum	Maximum
Al (%)	6.120	0.0100	0.0016	6.120	6.110	6.130
Cr (ppm)	144.167	0.9292	0.0064	144.600	143.100	144.800
Cu (ppm)	38.667	2.5166	0.0651	39.000	36.000	41.000
Fe (%)	0.227	0.0101	0.0444	0.228	0.216	0.236
Mo (ppm)	76.667	4.9329	0.0643	79.000	71.000	80.000
Ni (ppm)	198.667	6.1101	0.0308	200.000	192.000	204.000
Si (ppm)	163.333	15.2753	0.0935	160.000	150.000	180.000
Ti (%)	89.103	0.0153	0.0002	89.100	89.090	89.120
V (%)	4.376	0.0046	0.0010	4.377	4.371	4.380

SD — standard deviation; RSD — relative standard deviation.

Table 2
Basic statistical parameters for elemental concentrations determined in medical implant cobalt–chromium–molybdenum (CoCrMo) casting alloy (ISO 5832-4).

Element	Statistical parameter					
	Mean	SD	RSD	Median	Minimum	Maximum
Co (%)	65.140	0.1652	0.0025	65.150	64.970	65.300
Cr (%)	27.550	0.0300	0.0011	27.550	27.520	27.580
Cu (ppm)	188.300	0.7211	0.0038	188.100	187.700	189.100
Fe (%)	0.751	0.0078	0.0104	0.747	0.746	0.760
Mn (%)	0.726	0.0191	0.0264	0.720	0.710	0.747
Mo (%)	5.237	0.0379	0.0072	5.220	5.210	5.280
Ni (%)	0.495	0.0046	0.0093	0.498	0.490	0.498
Si (ppm)	577.933	5.0243	0.0087	575.600	574.500	583.700
Ti (ppm)	273.333	51.3160	0.1877	260.000	230.000	330.000
V (ppm)	733.333	40.4145	0.0551	740.000	690.000	770.000
Zn (ppm)	413.333	81.4453	0.1970	450.000	320.000	470.000

SD — standard deviation; RSD — relative standard deviation.

3.4. Induction of micronuclei, nucleoplasmic bridges and nuclear buds

The genotoxic activity of medical implant materials was further evaluated using CBMN assay. The induction of MNi, NPBs and NBUDs was assessed in binucleated lymphocytes (Fig. 1F–H). Although, exposure to all three hip joint replacement materials caused slightly higher number of CBMN assay parameters compared to negative control this difference was not statistically significant. When NDI was concerned there was no statistically significant difference between hip joint replacement materials and negative control for either of these parameters (Fig. 1I).

3.5. Correlations of tested parameters

The results of tail length showed high, statistically significant correlation with the percentage of viable cells after AO/EtBr ($r = -0.999$; $p = 0.0000$) and TB ($r = -0.996$; $p = 0.0000$) staining, as well as with total number of MNi ($r = 0.992$; $p = 0.0001$) and total number of NBUDs ($r = 0.996$; $p = 0.0000$). For other tested parameters there was no statistically significant correlation with tail length. Other two comet assay parameters did not show statistically significant correlation with other tested variables.

3.6. Particle morphology

The morphology of the particles was analyzed with an optical microscopy and with a SEM. SEM and optical microscopy images illustrate the particles external roughness. The particles are flat, sharp-edged, irregularly shaped grains with a side ratio ranging from 1:1 to 1:3. The mean particle sizes were less than 10 μm, and the size spectrum ranged for the particles from 1 μm up to about 300 μm. The percentile values of Ti_6Al_4V and CoCrMo alloy particle sizes from the optical microscopy (in silicon oil at 10× magnification) are presented in Tables 4 and 5. The diameter-to-length ratio (aspect ratio) of particles is an important shape characteristic relevant to the toxicological

Table 3
Basic statistical parameters for elemental concentrations determined in medical implant ultra high molecular weight polyethylene (ISO 5834-2).

Element (ppm)	Statistical parameter					
	Mean	SD	RSD	Median	Minimum	Maximum
Ca	5.213	0.0252	0.0048	5.210	5.190	5.240
Cr	17.213	0.0611	0.0035	17.200	17.160	17.280
Fe	7.143	0.0306	0.0043	7.150	7.110	7.170
Mn	4.533	0.0153	0.0034	4.530	4.520	4.550
Ni	2.867	0.0351	0.0123	2.870	2.830	2.900
Ti	5.340	0.0100	0.0019	5.340	5.330	5.350
Zn	3.683	0.0153	0.0041	3.680	3.670	3.700

SD — standard deviation; RSD — relative standard deviation.

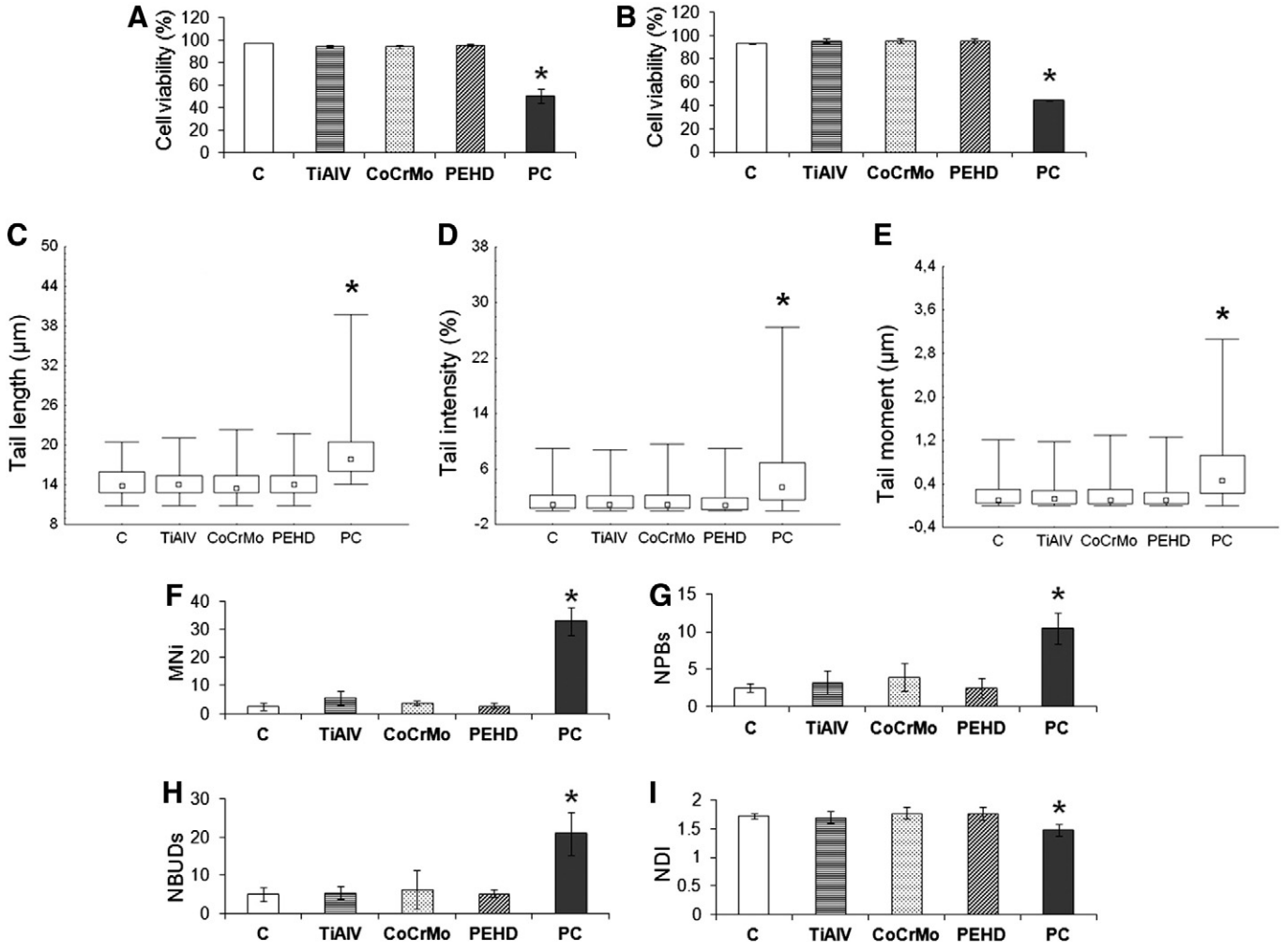

Fig. 1. The effects of medical implants particles on the viability, proliferation and DNA damage in HPBLs after the exposure to hip joint replacement materials (Ti_6Al_4V, CoCrMo and PEHD) for 24 h. Cell viability was determined by differential staining with AO/EtBr (A) and TB assay (B). DNA damage was assessed with the comet assay and is expressed as tail length (C), tail intensity (D) and tail moment (E). Incidence of MNi (F), NPBs (G) and NBUDs (H) as CBMN assay parameters were evaluated by analyzing binucleated cells while NDI (I) was evaluated by analyzing 500 cells. *$p < 0.05$. AO — acridine orange; C — control; CBMN — cytokinesis-block micronucleus; EtBr — ethidium bromide; MNi — micronuclei; NPBs — nucleoplasmic bridges; NBUDs — nuclear buds; NDI — nuclear division index; PC — positive control; TB — trypan blue.

property. Fibers are defined as elongated structures with an aspect ratio of 1:3 or greater. The Ti_6Al_4V particles are slightly more elongated and fibrous than the CoCrMo particles, and the PEHD particles are not elongated at all.

The size range of wear debris originating from implants corresponds to so-called "submicron wear" and produces a very large surface area per wear volume. This enables high reactivity with surrounding media and cellular elements. The metal alloy particle morphology, illustrated in Fig. 2 (Ti_6Al_4V and CoCrMo), is very similar to the collected wear debris particles. The surfaces of the Ti_6Al_4V and CoCrMo particles had visibly structured surfaces and are more irregular and granular than the PEHD particles surface (Fig. 2A–L). Fig. 3A–D presents the typical fingerprint of the metal alloys particles for the detection of Co, Cr and Mo. The co-presence of Co, Cr and Mo is a significant marker to identify the alloy (Fig. 3A–D). However energy dispersive X-ray analysis did not show any consistent differences in composition for the metal alloys particles within the limits of this technique (Fig. 4A and B).

3.7. Monofractal approaches: modified box counting method

The terms of the fractal analysis by the modified box counting method show generally a gradual decrease in the fractal dimensions ($D[B + BW]$ or $D[BW]$, $D[W + BW]$) of the surface with magnification of the SEM images, reflecting the disappearance of small features and observable particles (Fig. 5A–D) (Supplementary Fig. 1–3). This behavior is known and can be described in more general terms as fractal coarsening of the surface due to magnification. The strongest decrease in $D[BW]$ of the CoCrMo alloy particles with the magnification (Fig. 5B) has been observed at threshold level n = 16, and this dependence can be well described by a logarithmic function of magnification.

Table 4
Percentile values of Ti_6Al_4V alloy particle sizes from the optical microscopy (in silicon oil at 10× magnification); area (AECD) and perimeter (PECD) equivalent circular diameter.

Percentile (%)	Length (μm)	Width (μm)	Aspect ratio	AECD (μm)	PECD (μm)
10	3.28	1.64	1	4.14	1.6
50	13.32	5.59	1.8	8.15	8.47
90	278.93	170.06	3.4	165.21	324.98

Table 5
Percentile values of CoCrMo alloy particle sizes from the optical microscopy (in silicon oil at 10× magnification); area (AECD) and perimeter (PECD) equivalent circular diameter.

Percentile (%)	Length (μm)	Width (μm)	Aspect ratio	AECD (μm)	PECD (μm)
10	3.28	1.64	1	3.7	1.07
50	6.51	3.67	1.63	6.15	4.5
90	111.44	63.29	2.39	71.46	100.78

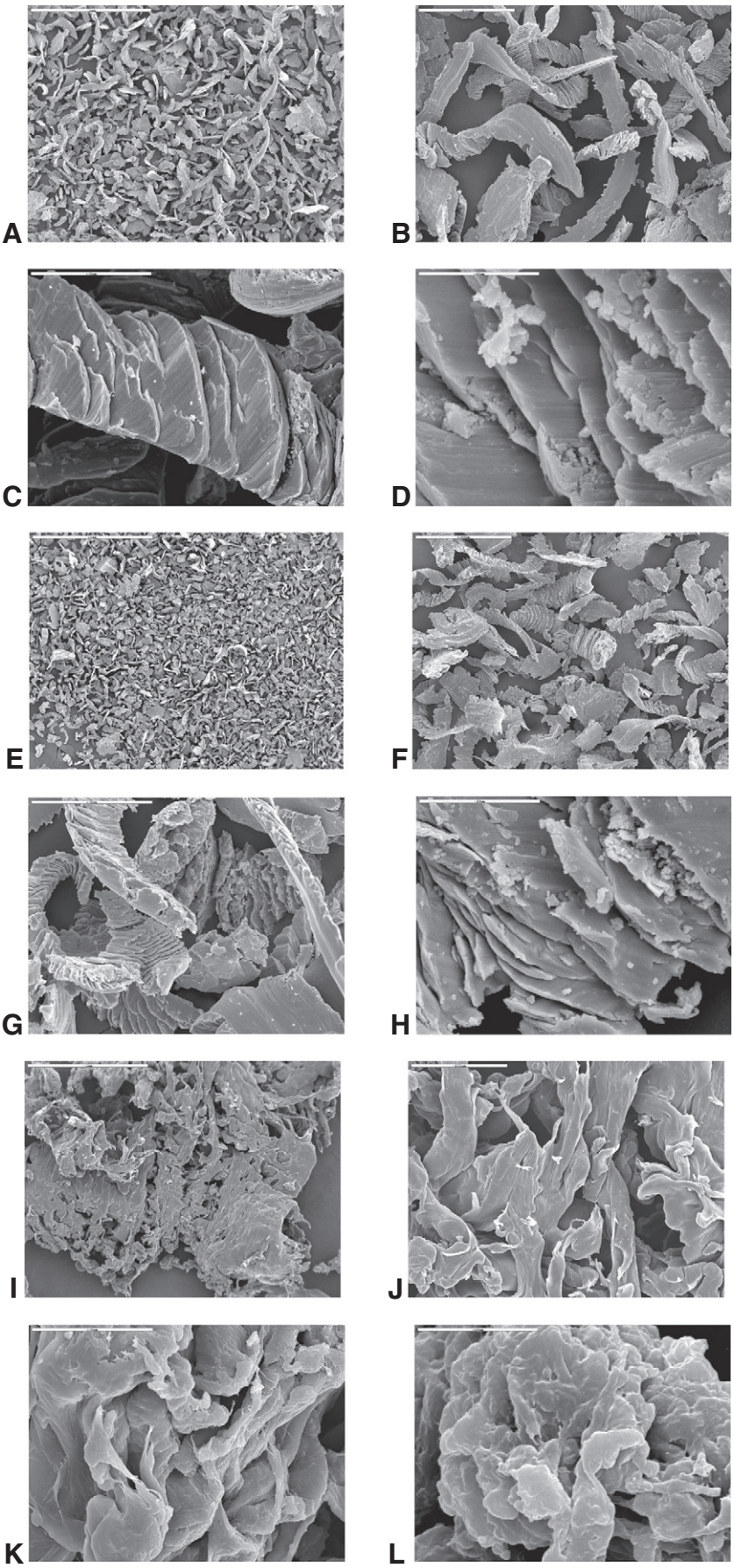

Fig. 2. Morphology of the Ti_6Al_4V (A–D), CoCrMo (E–H) and PEHD particles (I–L). SEM image (A, E, I) magnification 50×, scale bar 1 mm; (B, F, J) magnification 200×, scale bar 200 μm; (C, G, K) magnification 1000×, scale bar 50 μm; (D, H, L) magnification 5000×, scale bar 10 μm.

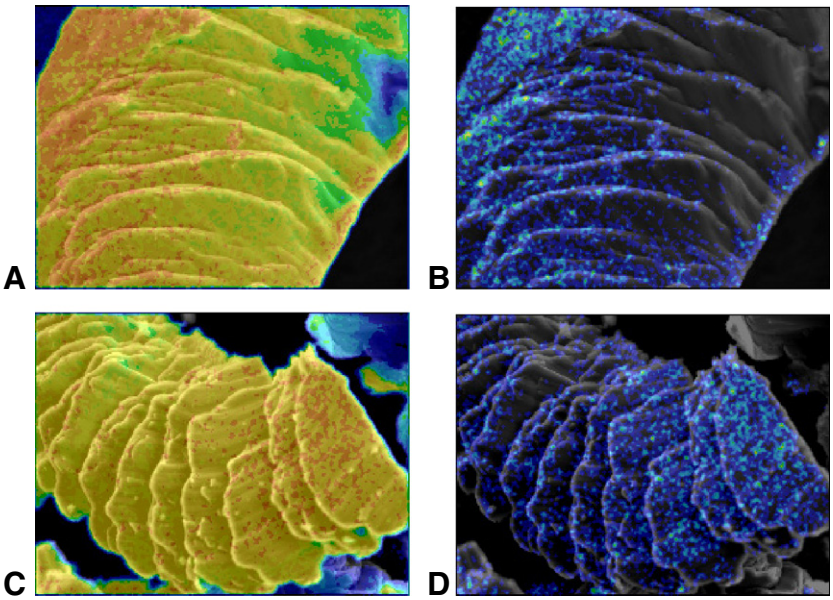

Fig. 3. Elemental mapping of the Ti_6Al_4V (A, B) and CoCrMo (C, D) particles.

The descriptive statistics relating to the distribution of fractal indices are shown in Table 6. The median interface fractal index $D[BW]$ (Fig. 6) is a linear decreasing function of the SEM magnification for all implant particles. The median box-counting fractal index $D[B + BW]$ does not significantly depend on the SEM magnification or the type of the implant particles (average $D[B + BW] = 1.973 \pm 0.04$). Clearly, there was an increase in irregularity for the metal alloys particles compared to the PEHD, not only in terms of the central tendency of the distribution of local connected fractal dimensions (mean and median), but also in terms of heterogeneity of the distribution of irregularities in the particle images (standard deviation). This increase is also shown in (Supplementary Figs. 4–14) as the fractal index distributions for the 3 implant materials.

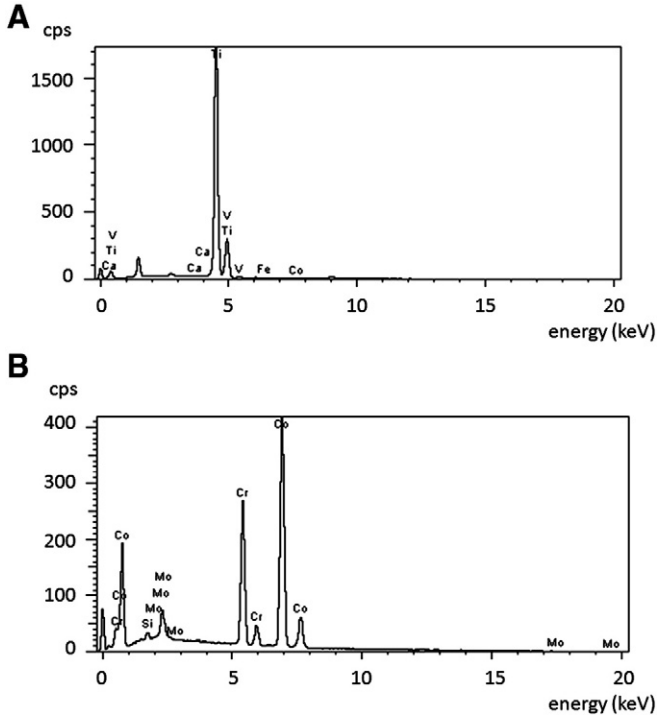

Fig. 4. Energy dispersive X-ray analysis (EDX) spectrum of the Ti_6Al_4V (A) and CoCrMo (B) particles.

3.8. Multifractal approach: generalized dimension

The results on the generalized correlation dimension $D(q)$ spectrum of implant particles SEM images are given in the Supplement (Supplementary Fig. 15–18; Supplementary Tables 1–4). The generalized fractal dimensions $D(q)$ spectrum is obtained by the Legendre transform of the $f(\alpha)$ singularity spectrum and it provides another representation of the multifractal spectrum.

3.8.1. Multifractal approach: multifractal spectra

The multifractal spectra $f(\alpha)$curves of implant particles SEM images at various magnifications follow typical convex shape of theoretical multifractal measures (Fig. 7A–D; Supplementary Fig. 19–21). General conclusion is that the parameters of multifractal analysis significantly differ for all three implant particles (Table 7). In this way, the starting hypothesis about these particles, that they are not different, is redrawn.

3.9. Lacunarity, Λ

Lacunarity Λ is an index for measuring the distribution of voids in a geometric object, with the object being more lacunar than others if its void sizes are distributed over a wider range. Geometric objects with relatively low lacunarity are homogeneous and translationally invariant. In contrast, objects with a wide range of void sizes are heterogeneous and non-translationally invariant; they have high lacunarity. The lacunarity pertains to both gaps and heterogeneity present in the SEM image, and the images that show greater variation and gaps have correspondingly higher lacunarities. The PEHD particles have the largest lacunarity, and the CoCrMo and Ti_6Al_4V metal alloys particles have lower lacunarity. The increase in the SEM magnification above 100× produces the image of the implant particles that corresponds more to the particle surface not to the particle shape, and then the lacunarity represents the heterogeneity of the particle surface. At magnification above 200×–500×, there is no difference in lacunarity among the various implant material particles (Table 8).

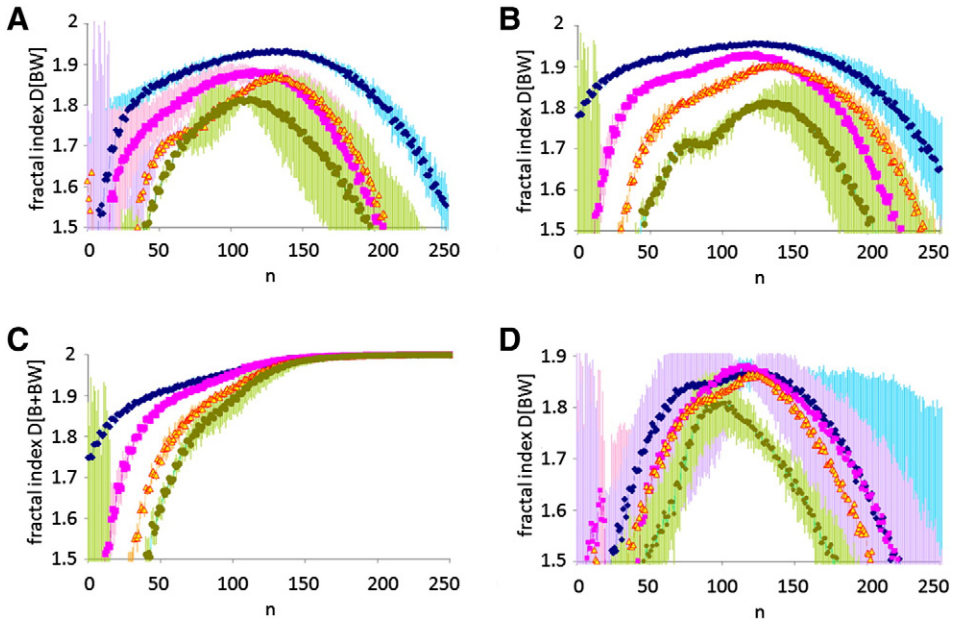

Fig. 5. Spectra of the fractal indices *D*[*BW*] (A), by the modified box counting method of Ti_6Al_4V particles as function of threshold (n); *D*[*BW*] (B) and *D*[*B* + *BW*] (C) by the modified box counting method of CoCrMo particles as function of threshold (n); *D*[*BW*] (D), by the modified box counting method of PEHD particles as function of threshold (n) at magnification 50× (♦), 100× (■) 200× (▲) and 500× (●).

4. Discussion

Large numbers of patients, especially young ones are receiving joint replacements and the number is constantly increasing. Several different artificial materials are used today in such procedures. Thus, present study aimed to evaluate chemical composition and possible cyto/genotoxicity of such medical implants. We used metal alloy (Ti_6Al_4V and CoCrMo) and PEHD particles to evaluate their impact in HPBLs *in vitro*. Titanium-based alloys are known to be the most corrosion resistant and biocompatible of all implant materials in the body. Pure titanium is preferably used for hip cup shells with polyethylene inserts. The high strength Ti_6Al_4V alloy is mainly used for anchorage stems of femoral components with wear-resistant CoCrMo metal or Al_2O_3 ceramic ball heads [34].

Results of EDXRF analysis showed that none of the elements identified in three hip joint parts deviate from the chemical composition defined by appropriate ISO standard. These results were in agreement with those obtained by X-ray elemental mapping. Additionally, toxicological characterization of tested particles did not show any cytotoxic or genotoxic potential on HPBLs in concentration tested.

Table 6
Median values of fractal indices at various scanning electron microscope (SEM) images magnifications.

Magnification	50×	100×	200×	500×
Fractal index				
Ti_6Al_4V				
D[*BW*]	1.8644	1.7437	1.7093	1.6063
D[*B* + *BW*]	1.9682	1.9745	1.9635	1.9776
D[*W* + *BW*]	1.9552	1.9025	1.9091	1.8270
CoCrMo				
D[*BW*]	1.9137	1.8388	1.7969	1.6245
D[*B* + *BW*]	1.9791	1.9817	1.9682	1.9575
D[*W* + *BW*]	1.9613	1.9308	1.9294	1.8719
PEHD				
D[*BW*]	1.7461	1.7024	1.6616	1.5102
D[*B* + *BW*]	1.9779	1.9784	1.9739	1.9802
D[*W* + *BW*]	1.8878	1.8915	1.8839	1.7885

PEHD — high density polyethylene.

The viability of HPBLs exposed to medical implant materials was not significantly affected determined with both vital staining using AO and EtBr, and TB exclusion assay. Several *in vitro* studies reported on toxicity of these particles on different cell models with the various results. TiAlV alloy reduced cell growth when in direct contact with rat fibroblasts [35], whereas they had no effect on HPBLs [36] or mouse fibroblasts [37] proliferation. CoCrMo alloy may also reduce cell growth when in direct contact with fibroblast cells [35] and inhibit lymphocyte proliferation [36].

As for the genotoxicity testing, none of the three determined comet assay parameters showed significant difference in the amount of DNA strand breaks compare to the unexposed samples. Additionally, CBMN assay parameters also proved that the tested materials were not genotoxic toward HPBLs in tested concentration. According to Katzer et al. [38,39] neither the bacterial nor the mammalian cell assays produced evidence of toxic or mutagenic effects in regard to both TiAlV and CoCrMo alloy exposure, therefore they are not to be expected to initiate carcinogenesis in the human organism. Similar results were provided by Assad et al. [40] where the cytotoxic and genotoxic activities of titanium-based alloy were not detected. The used TiAlV alloy for dental implants proved to be non-genotoxic which goes in line with our results and suggesting that titanium-based alloys should be used as long-term implants [37]. As for the PEHD, it is thought to be relatively immunologically inert material. In some studies it was even used as negative control [37], which implies that this material is

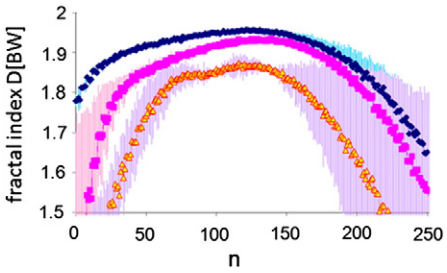

Fig. 6. Fractal index *D*[*BW*] spectrum (at various threshold n = 0–255) of implant particles SEM images at magnification 50×; CoCrMo (♦), Ti_6Al_4V (■) and PEHD particles (▲).

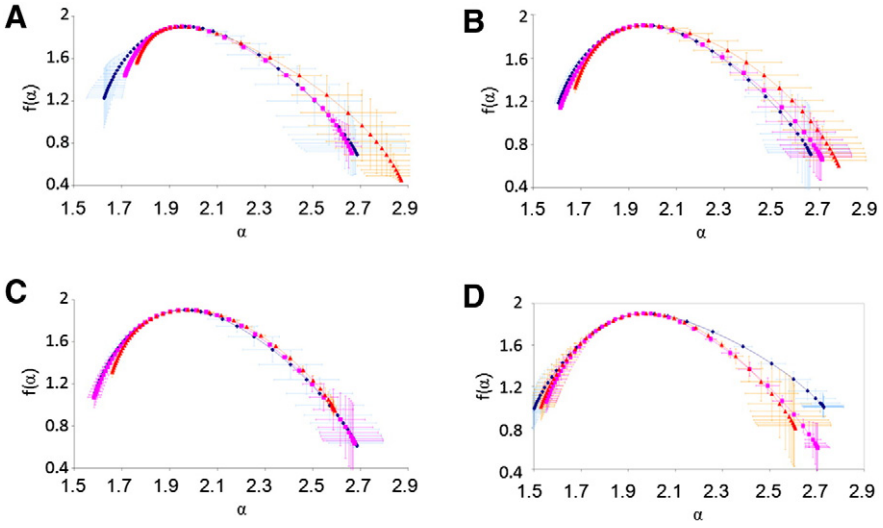

Fig. 7. Multifractal spectra of implant particles SEM images at magnification 50× (A), 100× (B), 200× (C), 500× (D) for CoCrMo (▲), Ti_6Al_4V (■) and PEHD particles (♦).

not cyto- or genotoxic [41–43], what was demonstrated in the present study as well.

Although modern implant materials have taken corrosion to the minimum, degradation of such materials can be expected [44–47] leading to the formation of metal wear nanoparticles that are released both from metal-on-metal and polyethylene-on-metal bearings, resulting in a postoperative increase in metal ion levels at different organ sites. These particles circulate both locally and systemically, penetrate cell plasma membranes, bind to cellular proteins and enzymes and modulate cytokine expression [48]. It should be highlighted that MOM implants can produce approximately 10^{12}–10^{14} alloy nanoparticles per year [49,50] and this phenomena is more characteristic to CoCrMo alloys. Higher concentrations of chromium and molybdenum have been found in liver and kidney tissue of Wistar rats that had implanted CoCr alloy-made wire, thus up-regulating metallothioneins [51]. Similar increase in concentrations of metals has been noticed in patients with total joint arthroplasty. Cobalt, chromium and titanium concentrations were higher in liver, spleen and pseudo-capsule tissue, while skeletal muscles and lung tissue had higher concentrations of Co, Cr and Ti, respectively [52].

Presence of heavy metals in human fibroblasts, amnion cells, and CHO K1 cell lines managed to induce genomic damage in some studies. Both CoCr and TiAlV alloys showed some genotoxic properties, as they produced DNA damage which resulted with the increase in frequency of chromosome aberrations, MNi, comet tail, and double stranded brakes using γ-H2AX foci assay [3,4,53–57].

Despite the fact that the surgical implants and other foreign bodies are listed as not carcinogenic to humans (group 3) according to International Agency for Research on Cancer (IARC), genotoxicity testing still produce contradictory results [58]. When implanted in the body, due to material degradation, the occurrence of alloy oxidation is possible, thus turning passive forms of titanium and chromium into more reactive ones [4]. Based on the same IARC classification, titanium oxide (TiO_2) is listed as possible human carcinogen, and chromium (VI) as human carcinogen [3,58–60]. Formation of more toxic metal forms could be one of the answers why some studies proved this alloys to be genotoxic.

Apart from the chemically induced cyto- and geno-toxicity, particle effect is another parameter that needs to be addressed. Alloy particle size varies from nanoscale [56] to microscale [3,4], and sometimes data of size and/or shape of the particles are not presented [53,54,57]. Particles tested here are micro-sized and some of the edges could be described as sharp. Despite the alloy shape and size, the cell viability of HPBLs remained above 90% which indicates that particle shape did not affect cell viability or the genotoxicity. However, the remaining toxicity corresponds to the change in the particle shape as measured by the fractal dimension. The implant materials with the prescribed chemical compositions have been shown to exhibit decreased cytotoxicity. The materials range in chemical composition and physicochemical properties. While physicochemical characteristics of the materials did not correlate with the observed trend in remnant cell viability, results from fractal analysis elucidate that the percent loss of cell viability can be correlated to morphology. Specifically, when the aggregate compactness, quantified by the fractal dimension, is taken, we find that highly compact characteristics of materials that result in reduced cytotoxicity.

Cell viability (TB method) is decreasing function of fractal dimensions $D[BW]$ (at n = 129 thresholds and at all magnifications) (Fig. 8A and B). The total number of NPBs is increasing function of fractal dimensions $D[BW]$ (Fig. 9A) (at n = 129 thresholds and at all magnifications). The total number of NBUDs is increasing function of fractal dimension $D[BW]$ (at n = 129 thresholds and at all magnifications) (Fig. 9B). Also, the total number of NPBs and NBUDs (Supplementary Fig. 22 and 23) is a decreasing function and, the cell viability (TB method) (Supplementary Fig. 24) is an increasing function of the lacunarity, Λ, especially at lower magnifications. The multifractal terms $\Delta f(\alpha)$ (Table 7) are related to the total number of

Table 7
Multifractal terms of implant particles scanning electron microscope (SEM) images.

Magnification	50×		100×		200×		500×	
	Δα	Δf(α)	Δα	Δf(α)	Δα	Δf(α)	Δα	Δf(α)
Ti_6Al_4V	0.9363	−0.6713	1.0921	−0.4570	1.0866	−0.4113	1.1496	−0.4391
CoCrMo	1.0991	−1.0758	1.0939	−0.6775	0.9286	−0.3483	1.0748	−0.1866
PEHD	1.0531	−0.5083	1.0529	−0.4596	1.0922	−0.4811	1.2300	0.0703

PEHD — high density polyethylene.

Table 8
Lacunarity Λ of the implant particles scanning electron microscope (SEM) images.

Magnification	50×		100×		200×		500×	
	Λ	SD	Λ	SD	Λ	SD	Λ	SD
Ti_6Al_4V	0.126	0.000	0.183	0.012	0.230	0.009	0.284	0.038
CoCrMo	0.092	0.001	0.166	0.010	0.203	0.019	0.311	0.046
PEHD	0.224	0.007	0.243	0.018	0.231	0.037	0.321	0.020

PEHD — high density polyethylene; SD — standard deviation.

NPBs and NBUDs, and to the cell viability (TB method; Fig. 9C and D) up to the 200× magnification. The multifractal width terms Δα (Table 7) are weakly related to the total number of NPBs, NBUDs and to the cell viability (TB method) only at higher magnifications (at magnifications > 200×) (Supplementary Fig. 25).

Results registered after measuring the fractal dimension of the implant metal alloys and polyethylene particles shape and the induced genotoxicity in HPBLs have shown significant differences between various implants. Irregularity of particles outlines by *D*[*BW*] was found to have a higher value in the implant metal alloys than in the polyethylene particles. The increased particle fractal index *D*[*BW*] found in the implant metal alloys particles is the mathematical equivalent of a higher complexity of the particle architecture. Explanations of our findings as represented by the lower cell viability (TB method) and the mean frequency of CBMN assay parameter (NPBs) in HPBLs of metal alloys particles is that these are affected by the self-similarity of the structures across different scales. The growth patterns of cell lines can be characterized using the fractal dimension [61]. Analyzing the generalized fractal dimension (D(q), see Supplement) and its Legendre transform $f(\alpha)$ revealed that under implant conditions, all multifractal parameters determined had values greater for PEHD compared with metallic implants, consistent with cell viability effects. All fractal parameters studied were sensitive to the cell viability (TB method) and the mean frequency of CBMN assay parameter (NPBs) in HPBLs.

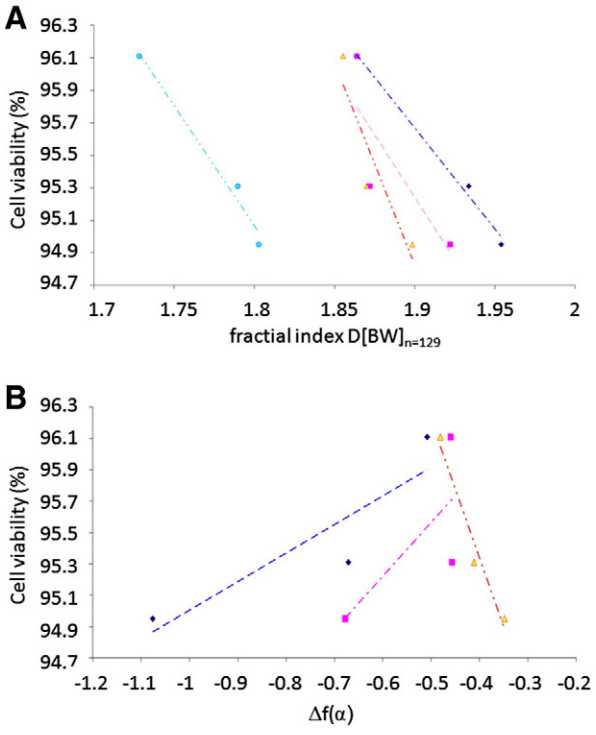

Fig. 8. Cell viability (TB method) relation with the fractal dimensions *D*[*BW*] (at n = 129 thresholds) (A) and with the multifractal difference term $\Delta f(\alpha)$ (B) at magnifications ♦ 50×, ■ 100×, ▲ 200×, ● 500×.

However, no the significant difference or trend on the fractal-dependent toxic effects as determined by the cell viability (AO/EtBr method) nor by the frequency of CMBN assay parameters such as the MNi and NDI for the alloys and plastic particles.

It should be also highlighted that chromium-based powder is positioned in possible human carcinogens [58] what could have been the reason for aberrations detected in some studies. It has to be pointed out that all discussed studies investigated short-term effects of tested alloys with time exposures ranging from 6 to 120 h. Generally, hip implants are life-long, and exist in complex environment. In the future, studies evaluating cytogenetic status of the patients with replaced hips could bring evidence of long-term effects that this materials may have on genome instability and human health in total.

One such study was done by Coen et al. [53] where wear debris was extracted from patients with total hip replacements. Approximately 6.4 g of TiAlV alloy was detected in tissue near artificial hip. After making series of dilutions, they have demonstrated that concentration of 12.5 μg/ml raised the number of aberrant chromosomes. Similar, although slightly lower concentration (10 μg/ml) was used in the present study to test cyto/genotoxic potential of PEHD, TiAlV, and CoCrMo alloy. Other studies discussed above that detected cyto- and genotoxicity of such materials had even higher concentrations than the one tested in the present study. Interesting aspect of lowering genotoxicity of CoCrMo alloy is macrophage activity. Natural detoxification of CoCrMo alloy is a process that can normally be expected in tissues near hip replacements. Fibroblasts exposed to CoCrMo alloy *in vitro* resulted with increase of comet tail moment, and decrease of cell viability. After macrophage detoxification such effects failed to be observed [62].

5. Conclusions

In conclusion, orthopedic implants produced of Ti_6Al_4V, CoCrMo and PEHD proved to be non-cytotoxic and non-genotoxic, in tested concentration. Nevertheless, taking in to account the abovementioned studies there is a constant need for monitoring of patients that have implanted artificial hips or other joints, therefore minimizing risks of any unwanted health effects. Because there are studies that suggest that these alloys could be harmful, development of new and improved materials can be expected. Primarily, new materials should be more stabile thus eliminating possibility of alloy degradation which could be considered as the most important source of potential toxicity.

There was significant difference between the various degrees of cell viability and assay with the boundary fractal index *D*[*BW*] of implant metal alloys and polyethylene particles. Fractal analysis may contribute to the assessment of genotoxicity of implant metal alloys and polyethylene particles in human lymphocytes. Higher values of fractal indices *D*(*BW*) are directly associated with progressively lower degrees of genotoxicity implant metal alloys and polyethylene particles in human lymphocytes. A surface property of biomaterial implants that communicates with its environment is directly related to *in vitro* biological performance such as cell growth. An important goal in the use of biocompatible materials is to create surfaces that minimize non-specific interactions with cells.

Conflict of interests

The authors declare that there have been no conflicts of interests in this research.

Acknowledgements

This work was supported by the Croatian Ministry of Science, Education and Sports (Grant no. 022-0222148-2125).

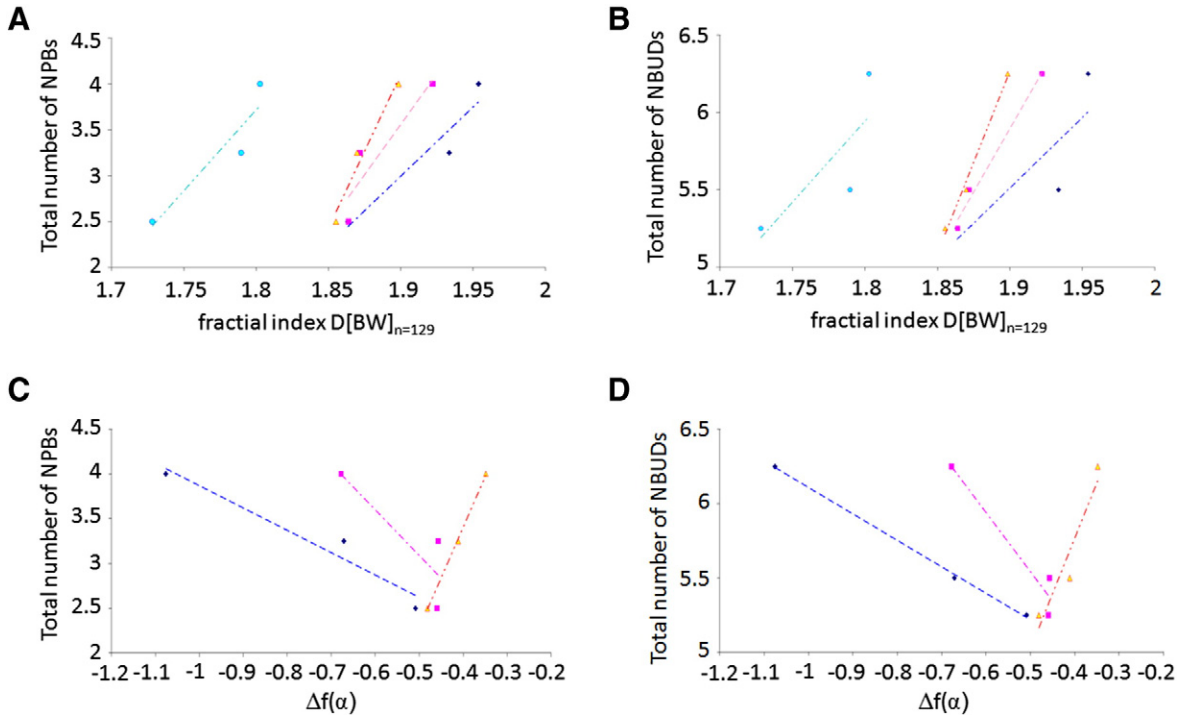

Fig. 9. Total number of NPBs (A) and NBUDs (B) relation with the fractal dimensions *D*[*BW*] (at n = 129 thresholds), and total number of NPBs (C) and NBUDs (D) relation with the multifractal difference term $\Delta f(\alpha)$ at magnifications ♦ 50×, ■ 100×, △ 200×.

Appendix A. Supplementary data

Supplementary data to this article can be found online at http://dx.doi.org/10.1016/j.bbagen.2013.10.015.

References

[1] G. Garellick, H. Malchau, P. Herberts, E. Hansson, H. Axelsson, T. Hansson, Life expectancy and cost utility after total hip replacement, Clin. Orthop. Relat. Res. 346 (1998) 141–151.
[2] N.N. Mahomed, J.A. Barrett, J.N. Katz, C.B. Phillips, E. Losina, R.A. Lew, E. Guadagnoli, W.H. Harris, R. Poss, J.A. Baron, Rates and outcomes of primary and revision total hip replacement in the United States medicare population, J. Bone Joint Surg. Am. 85 (2003) 27–32.
[3] I. Papageorgiou, Z. Yin, D. Ladon, D. Baird, A.C. Lewis, A. Sood, R. Newson, I.D. Learmonth, C.P. Case, Genotoxic effects of particles of surgical cobalt chrome alloy on human cells of different age in vitro, Mutat. Res. 619 (2007) 45–58.
[4] A. Tsaousi, E. Jones, C.P. Case, The in vitro genotoxicity of orthopaedic ceramic (Al_2O_3) and metal (CoCr alloy) particles, Mutat. Res. 697 (2010) 1–9.
[5] W. Wang, Y. Ouyang, C.K. Poh, Orthopaedic implant technology: biomaterials from past to future, Ann. Acad. Med. Singapore 40 (2011) 237–238.
[6] T.P. Schmalzried, J.J. Callaghan, Wear in total hip and knee replacements, J. Bone Joint Surg. Am. 81 (1999) 115–136.
[7] H. Bhatt, T. Goswami, Implant wear mechanisms—basic approach, Biomed. Mater. 3 (2008) 042001.
[8] V. Trkulja, R. Kolundzic, Rivaroxaban vs dabigatran for thromboprophylaxis after joint-replacement surgery: exploratory indirect comparison based on meta-analysis of pivotal clinical trials, Croat. Med. J. 51 (2010) 113–123.
[9] N. Nomura, Artificial organs: recent progress in metals and ceramics, J. Artif. Organs 13 (2010) 10–12.
[10] R. Tuli, J. Parvizi, Alternative bearing surfaces in total hip arthroplasty, Expert Rev. Med. Devices 2 (2005) 445–452.
[11] L.V. Wilches, J.A. Uribe, A. Toro, Wear of materials used for artificial joints in total hip replacements, Wear 265 (2008) 143–149.
[12] C.P. Case, V.G. Langkamer, R.T. Howell, J. Webb, G. Standen, M. Palmer, A. Kemp, I.D. Learmonth, Preliminary observations on possible premalignant changes in bone marrow adjacent to worn total hip arthroplasty implants, Clin. Orthop. Relat. Res. 329 (1996) 269–279.
[13] E. Ingham, J. Fisher, Biological reactions to wear debris in total joint replacement, Proc. Inst. Mech. Eng. H. 214 (2000) 21–37.
[14] A.T. Doherty, R.T. Howell, L.A. Ellis, I. Bisbinas, I.D. Learmonth, R. Newson, C.P. Case, Increased chromosome translocations and aneuploidy in peripheral blood lymphocytes of patients having revision arthroplasty of the hip, J. Bone Joint Surg. Br. 83 (2001) 1075–1081.
[15] C. Vermes, R. Chandrasekaran, J.J. Jacobs, J.O. Galante, K.A. Roebuck, T.T. Glant, The effects of particulate wear debris, cytokines, and growth factors on the functions of MG-63 osteoblasts, J. Bone Joint Surg. Am. 83 (2001) 201–211.
[16] D. Ladon, A. Doherty, R. Newson, J. Turner, M. Bhamra, C.P. Case, Changes in metal levels and chromosome aberrations in the peripheral blood of patients after metal-on-metal hip arthroplasty, J. Arthroplasty 19 (2004) 78–83.
[17] A.P. Davies, A. Sood, A.C. Lewis, R. Newson, I.D. Learmonth, C.P. Case, Metal-specific differences in levels of DNA damage caused by synovial fluid recovered at revision arthroplasty, J. Bone Joint Surg. Br. 87 (2005) 1439–1444.
[18] N.P. Singh, Microgels for estimation of DNA strand breaks, DNA protein crosslinks and apoptosis, Mutat. Res. 455 (2000) 111–127.
[19] R.C. Duke, J.J. Cohen, Morphological and biochemical assays of apoptosis, in: J.E. Coligan, A.M. Kruisbeal (Eds.), Current Protocols in Immunology, John Willey & Sons, New York, 1992, pp. 1–3.
[20] W. Strober, Trypan blue exclusion test of cell viability, Curr. Protoc. Immunol. A3 (2001) A3B.
[21] N.P. Singh, M. McCoy, R. Tice, E. Schneider, A simple technique for quantitation of low levels of DNA damage in individual cells, Exp. Cell Res. 175 (1988) 184–191.
[22] G. Gajski, V. Garaj-Vrhovac, V. Oreščanin, Cytogenetic status and oxidative DNA-damage induced by atorvastatin in human peripheral blood lymphocytes: standard and Fpg-modified comet assay, Toxicol. Appl. Pharmacol. 231 (2008) 85–93.
[23] M. Fenech, A.A. Morley, Measurement of micronuclei in lymphocytes, Mutat. Res. 147 (1985) 29–36.
[24] M. Fenech, W.P. Chang, M. Kirsch-Volders, N. Holland, S. Bonassi, E. Zeiger, HUMN project: detailed description of scoring criteria for the cytokinesis-block micronucleus assay using isolated human lymphocyte cultures, Mutat. Res. 534 (2003) 65–75.
[25] M. Kirsch-Volders, T. Sofuni, M. Aardema, S. Albertini, D. Eastmond, M. Fenech, M. Ishidate Jr., S. Kirchner, E. Lorge, T. Morita, H. Norppa, J. Surrallés, A. Vanhauwaert, A. Wakata, Report from the in vitro micronucleus assay working group, Mutat. Res. 540 (2003) 153–163.
[26] G. Landini, Y. Hirayama, T.J. Li, M. Kitano, Increased fractal complexity of the epithelial–connective tissue interface in the tongue of 4NQO-treated rats, Pathol. Res. Pract. 196 (2000) 251–258.
[27] http://www.fch.vutbr.cz/lectures/imagesci/(accessed 13.02.2012.).
[28] A. Karperien, A. Karperien, FracLac for ImageJ, version 2.5, http://rsb.info.nih.gov/ij/plugins/fraclac/FLHelp/Introduction.htm(accessed 13.02.2012.).
[29] T.C. Halsey, M.H. Jensen, L.P. Kadanoff, I. Procaccia, B.I. Shraiman, Fractal measures and their singularities: the characterization of strange sets, Phys. Rev. A 33 (1986) 1141–1151.
[30] T. Vicsek, Mass multifractals, Physica A 168 (1990) 490–497.
[31] A. Chhabra, R.V. Jensen, Direct determination of the f(alpha) singularity spectrum, Phys. Rev. Lett. 62 (1989) 1327–1330.
[32] L. Henderson, A. Wolfreys, J. Fedyk, C. Bourner, S. Windebank, The ability of the Comet assay to discriminate between genotoxins and cytotoxins, Mutagenesis 13 (1998) 89–94.

[33] R.R. Tice, E. Agurell, D. Anderson, B. Burlinson, A. Hartmann, H. Kobayashi, Y. Miyamae, E. Rojas, J.C. Ryu, Y.F. Sasaki, Single cell gel/comet assay: guidelines for in vitro and in vivo genetic toxicology testing, Environ. Mol. Mutagen. 35 (2000) 206–221.
[34] M. Semlitsch, Titanium alloys for hip joint replacements, Clin. Mater. 2 (1987) 1–13.
[35] E.J. Evans, Cell damage in vitro following direct contact with fine particles of titanium, titanium alloy and cobalt–chrome–molybdenum alloy, Biomaterials 15 (1994) 713–717.
[36] C. Faleiro, I. Godinho, U. Reus, M. de Sousa, Cobalt–chromium–molybdenum but not titanium–6aluminium–4vanadium alloy discs inhibit human T cell activation in vitro, Biometals 9 (1996) 321–326.
[37] E. Velasco-Ortegaa, A. Jos, A.M. Cameánb, J. Pato-Moureloa, J.J. Segura-Egeaa, In vitro evaluation of cytotoxicity and genotoxicity of a commercial titanium alloy for dental implantology, Mutat. Res. 702 (2010) 17–23.
[38] A. Katzer, S. Hockertz, G.H. Buchhorn, J.F. Loehr, In vitro toxicity and mutagenicity of CoCrMo and Ti_6Al wear particles, Toxicology 190 (2003) 145–154.
[39] A. Katzer, G.H. Buchhorn, S. Hockertz, J.F. Loehr, In vitro toxicity and mutagenicity of CoCrMo and TiAl wear particles, Orthopade 32 (2003) 744–750.
[40] M. Assad, A. Chernyshov, M.A. Leroux, C.H. Rivard, A new porous titanium-nickel alloy: part 1. Cytotoxicity and genotoxicity evaluation, Biomed. Mater. Eng. 12 (2002) 225–237.
[41] P.F. Doorn, P.A. Campbell, H.C. Amstutz, Metal versus polyethylene wear particles in total hip replacements. A review, Clin. Orthop. Relat. Res. 329 (1996) 206–216.
[42] E.B. Benz, M. Federman, J.J. Godleski, B.E. Bierbaum, T.S. Thornhill, M. Spector, Transmission electron microscopy of intracellular particles of polyethylene from joint replacement prostheses: size distribution and cellular response, Biomaterials 22 (2001) 2835–2842.
[43] H. Fouad, R. Elleithy, High density polyethylene/graphite nano-composites for total hip joint replacements: processing and in vitro characterization, J. Mech. Behav. Biomed. Mater. 4 (2011) 1376–1383.
[44] M. Böhler, F. Kanz, B. Schwarz, I. Steffan, A. Walter, H. Plenk Jr., K. Knahr, Adverse tissue reactions to wear particles from Co-alloy articulations, increased by alumina-blasting particle contamination from cementless Ti-based total hip implants. A report of seven revisions with early failure, J. Bone Joint Surg. Br. 84 (2002) 128–136.
[45] J. Komotori, N. Hisamori, Y. Ohmori, The corrosion/wear mechanisms of Ti–6Al–4V alloy for different scratching rates, Wear 263 (2007) 412–418.
[46] A. Buford, T. Goswami, Review of wear mechanisms in hip implants: Paper I – General, Mater. Des. 25 (2004) 385–393.
[47] G. Manivasagam, D. Dhinasekaran, A. Rajamanickam, Biomedical implants: corrosion and its prevention — a review, Recent Pat. Corros. Sci. 2 (2010) 40–54.
[48] I. Polyzois, D. Nikolopoulos, I. Michos, E. Patsouris, S. Theocharis, Local and systemic toxicity of nanoscale debris particles in total hip arthroplasty, J. Appl. Toxicol. 32 (2012) 255–269.
[49] P.F. Doorn, P.A. Campbell, J. Worrall, P.D. Benya, H.A. McKellop, H.C. Amstutz, Metal wear particle characterization from metal on metal total hip replacements: transmission electron microscopy study of periprosthetic tissues and isolated particles, J. Biomed. Mater. Res. 42 (1998) 103–111.
[50] C. Brown, S. Williams, J.L. Tipper, J. Fisher, E. Ingham, Characterisation of wear articles produced by metal on metal and ceramic on metal hip prostheses under standard and microseparation simulation, J. Mater. Sci. Mater. Med. 18 (2007) 819–827.
[51] S.S. Jakobsen, G. Danscher, M. Stoltenberg, A. Larsen, J.M. Bruun, T. Mygind, K. Kemp, K. Soballe, Cobalt–chromium–molybdenum alloy causes metal accumulation and metallothionein up-regulation in rat liver and kidney, Basic Clin. Pharmacol. Toxicol. 101 (2007) 441–446.
[52] N.J. Hallab, K. Mikecz, C. Vermes, A. Skipor, J.J. Jacobs, Orthopaedic implant related metal toxicity in terms of human lymphocyte reactivity to metal–protein complexes produced from cobalt-base and titanium-base implant alloy degradation, Mol. Cell. Biochem. 222 (2001) 127–136.
[53] N. Coen, M.A. Kadhim, E.G. Wright, C.P. Case, C.E. Mothersill, Particulate debris from a titanium metal prosthesis induces genomic instability in primary human fibroblast cells, Br. J. Cancer 88 (2003) 548–552.
[54] B. Daley, A.T. Doherty, B. Fairman, C.P. Case, Wear debris from hip or knee replacements causes chromosomal damage in human cells in tissue culture, J. Bone Joint Surg. Br. 86 (2004) 598–606.
[55] I. Papageorgiou, C. Brown, R. Schins, S. Singh, R. Newson, S. Davis, J. Fisher, E. Ingham, C.P. Case, The effect of nano- and micron-sized particles of cobalt–chromium alloy on human fibroblasts in vitro, Biomaterials 28 (2007) 2946–2958.
[56] M.C. Parry, G. Bhabra, A. Sood, F. Machado, L. Cartwright, M. Saunders, E. Ingham, R. Newson, A.W. Blom, C.P. Case, Thresholds for indirect DNA damage across cellular barriers for orthopaedic biomaterials, Biomaterials 31 (2010) 4477–4483.
[57] C.C. Gomes, L.M. Moreira, V.J. Santos, A.S. Ramos, J.P. Lyon, C.P. Soares, F.V. Santos, Assessment of the genetic risks of a metallic alloy used in medical implants, Genet. Mol. Biol. 34 (2011) 116–121.
[58] International Agency for Research on Cancer, Agents Reviewed by the IARC Monographs, vol. 1–100ALyon, France, 2009.
[59] M. Skocaj, M. Filipic, J. Petkovic, S. Novak, Titanium dioxide in our everyday life; is it safe? Radiol. Oncol. 45 (2011) 227–247.
[60] J.J. Wang, B.J.S. Sanderson, H. Wang, Cyto- and genotoxicity of ultrafine TiO_2 particles in cultured human lymphoblastoid cells, Mutat. Res. 628 (2007) 99–106.
[61] M.J. Vilela, M.L. Martins, S.R. Boschetti, Fractal patterns for cells in culture, J. Pathol. 177 (1995) 103–107.
[62] I. Papageorgiou, V. Shadrick, S. Davis, L. Hails, R. Schins, R. Newson, J. Fisher, E. Ingham, C.P. Case, Macrophages detoxify the genotoxic and cytotoxic effects of surgical cobalt chrome alloy particles but not quartz particles on human cells in vitro, Mutat. Res. 643 (2008) 11–19.